

A MEG Study of Different Motor Imagery Modes in Untrained Subjects for BCI Applications

Alexander E. Hramov¹^a, Elena N. Pitsik¹^b, Parth Chholak², Vladimir A. Maksimenko¹^c,
Nikita S. Frolov¹^d, Semen A. Kurkin¹^e and Alexander N. Pisarchik^{1,2}^f

¹Neuroscience and Cognitive Technology Laboratory, Innopolis University, 1 Universitetskaya str., Innopolis, 420500, The Republic of Tatarstan, Russia

²Center for Biomedical Technology, Technical University of Madrid, Campus Montegancedo, 28223 Pozuelo de Alarcón, Madrid, Spain

Keywords: Brain-computer Interface, MEG, Motor Imagery, Exoskeleton, HCA, Artificial Neural Network, Wavelet Analysis.

Abstract: Motor imagery is a most commonly studied neurophysiological pattern that is used in brain-computer interfaces as a command for exoskeletons, bioprostheses, wheelchair and other robotic devices. The mechanisms of motor imagery manifestation in human brain activity include dynamics of motor-related frequency bands in various brain areas, among which the most common is sensorimotor rhythm. In present work we consider time-frequency structure of magnetoencephalographical (MEG) motor imagery in untrained subjects. We conduct series of experiments to collect MEG motor imagery dataset in untrained subjects. We confirm the emergence of two types of motor imagery – visual (VI) and kinesthetic (KI), which cause different types of event-related potentials (ERP) dynamics and require different approaches to classification using machine learning methods. We also reveal the impact of dataset optimization on the artificial neural network performance, which is essential topic in brain-computer interface (BCI) development. We show that developing classification strategy based on time-frequency features of the particular MEG signal can increase classification accuracy of the VI mode to the level of the KI.

1 INTRODUCTION

Known brain-computer interfaces (BCIs) applications under study include: mental control of robotic devices such as exoskeletons and prostheses for people with motor disabilities, which allows to perform basic tasks such as relocation in a wheelchair, limbs movement etc. (Mirza et al., 2015); real-time recognition of cognitive activity, i.e. emotions, alertness and concentration (Victorino et al., 2015), which is widely used in support systems for education and professional skills training; neurofeedback for rehabilitation based on motor imagery (Yu et al., 2015). The focus of this study is *active BCIs*, which provide feedback to the user based on the brain activity measure-

ments and feature extraction in order to alter this activity in the "right direction" (Nijboer et al., 2009). The most widely used pattern is motor imagery (MI) for application in BCI for exoskeleton or robotic control (Frolov et al., 2017; Meng et al., 2016). Recognition and classification of MI using artificial intelligence methods is a challenging task, despite that some of the features of this pattern are well-known.

Sensorimotor rhythm (SMR) is perhaps the most common in the scientific literature in the context of motor imagery application in BCI (McFarland and Wolpaw, 2005; Kübler et al., 2005). SMR is an oscillatory idle rhythm of synchronized electromagnetic brain activity. It appears in spindles in recordings of EEG, MEG, and ECoG with the frequency range of 7 – 13 Hz (Arroyo et al., 1993). SMR training for BCI is widely employed technique for BCI-based therapy, which often includes muscle stimulation or exoskeleton control (Norman et al., 2018). Any motor action, including real movements, motor preparation and motor imagery, are resulting in changes in

^a <https://orcid.org/0000-0003-2787-2530>

^b <https://orcid.org/0000-0003-1850-2394>

^c <https://orcid.org/0000-0002-4632-6896>

^d <https://orcid.org/0000-0002-2788-1907>

^e <https://orcid.org/0000-0002-3438-5717>

^f <https://orcid.org/0000-0003-2471-2507>

SMR dynamics: so-called event-related desynchronization and synchronization (ERD/ERS). It is necessary to emphasize that real motor action is not required for changes in the SMR amplitude (Yi et al., 2016; Öztürk and Yilmaz, 2018). The user of the BCI can train to generate ERD or ERS in SMR (Penaloza et al., 2018; Tacchino et al., 2017) in response for external stimulation, which can be biological feedback integrated in BCI.

One of the most important problem which accompanies the development of SMR-based BCI is the variability of the neural activity from one subject to another (Ferreira et al., 2008; Ranky and Adamovich, 2010; Murphy et al., 2017). This variability is especially well pronounced in case of untrained subjects, because such BCI user may try different ways to perform MI without knowing which one of them BCI will "understand". It is known that training can partially resolve this issue (Duann and Chiou, 2016). The other possible solution is to use additional information about the nature of the signals. Recently, the practice of dividing MI modes on visual (VI) or kinesthetic imagery (KI) has become widespread (La Touche et al., 2018; Mehler et al., 2019a). These two perspectives are significantly different and are pronounced in neurophysiological activity in different ways (Filgueiras et al., 2018): during the VI, the subject imagines him/herself performing an action from the from the third-person point of view, or "looks throughout his/her own eyes" (Callow et al., 2017). During the KI the subject imagines the feeling and experience of movements without overt movement (Mehler et al., 2019b; Hanakawa, 2016).

In present work, we consider time-frequency structure of the MEG signal corresponding to these two MI modes in untrained subjects. We evaluate changes in event-related potentials amplitude in sensorimotor rhythm, particularly focusing on μ - and β -frequency bands, where ERD during motor activity emerges (Duann and Chiou, 2016; Maksimenko et al., 2018). Then, we applied machine learning algorithms to detect clusters among selected features and then check how different frequency components affect the artificial neural networks performance. The results and observations focused in present paper provide the deeper insight into the VI and KI modes of motor imagery and allow us to implement an optimal classification approach for both groups of subjects.

2 METHODS

2.1 Experimental Setup and Data Preparation

First, we performed series of experiments to collect magnetoencephalographical (MEG) MI dataset in untrained subjects. All experimental work was conducted using the equipment of the Laboratory of Cognitive and Computational Neuroscience (CTB, Technical University of Madrid, Spain). Seven volunteers in age of 20–31 participated in the experimental study. During the experimental sessions, participants were sitting in the chair in the comfortable posture, which allows to minimize any motor activity throughout the experiment. A screen was installed in front of the chair, which is used to transmit commands at each stage of the experiment. To divide one trial from another, audio signals were tuned on at random intervals of 6-8 seconds.

The whole experimental session consisted of four parts, each part included equal number of left or right arm motor imagery tasks. Each part was preceded by the announcement on the screen in front of the subject, and short audio signals was informing subjects about the trial start.

306-channel (204 planar gradiometers and 102 magnetometers) MEG-recordings with sampling frequency 1000 Hz was collected using Vectorview MEG system (Elekta AB, Stockholm, Sweden). An online anti-alias filter with cutoffs between 0.1 Hz and 300 Hz was applied. Further preparations of the data was conducted using Brainstorm application for MATLAB and included selection of 5-seconds trials corresponding to each motor imagery task and 20-seconds fragments corresponding to the resting state with closed eyes according to the experimental protocol.

2.2 Time-frequency Wavelet-based Analysis

We used wavelet-based approach to perform time-frequency analysis of obtained data. For each MEG-channel $X_n(t)$ the wavelet energy spectrum was calculated:

$$E^n(f, t) = \sqrt{W_n(f, t)^2} \quad (1)$$

where $W_n(f, t)$:

$$W_n(f, t) = \sqrt{f} \int_{t-\frac{4}{f}}^{t+\frac{4}{f}} X_n(t) \Psi^*(f, t) dt, \quad (2)$$

is complex-valued wavelet coefficients with MEG channel number $n = 1, \dots, 102$, * standing for complex conjugation and $\psi(f, t)$ is a mother wavelet function, which in our case is the Morlet wavelet with central frequency $\omega_0 = 2\pi$, $f_0 = 2\pi$:

$$\psi(f, t) = \sqrt{f}\pi^{1/4} e^{j\omega_0 f(t-t_0)} e^{f(t-t_0)^2/2}, \quad (3)$$

Morlet wavelet is often used in medicine for analysis of neurological data and a heartbeat behaviour (Morlet et al., 1993).

Since we considering ERP in the context of motor imagery, we calculated values of wavelet energy $E_\mu^n(t)$ and $E_\beta^n(t)$ for each channel n in frequency bands β (8–13 Hz), and μ (15–30 Hz), where ERD and ERS are well-known to be observed during both real and imagery motor activity:

$$E_{\mu,\beta}^n(t) = \frac{1}{\Delta f} \int_{f \in \mu,\beta} E^n(f, t) df. \quad (4)$$

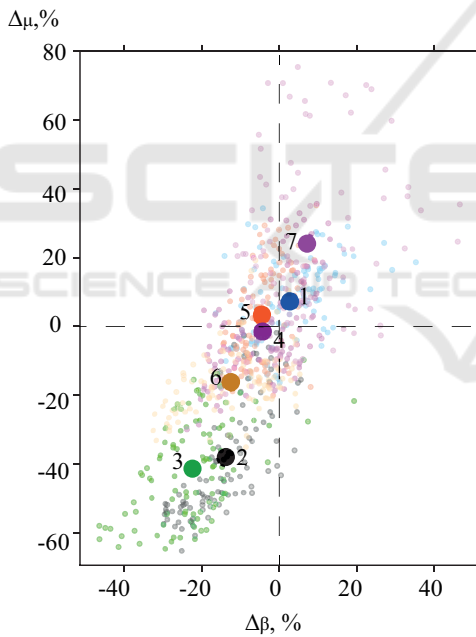


Figure 1: MI wavelet energy differences for each of 7 subjects.

The values of ERP for each type of trial, i.e. left hand ($L_\mu^n(t)$ and $L_\beta^n(t)$), right hand ($R_\mu^n(t)$ and $R_\beta^n(t)$) and resting state ($B_\mu^n(t)$ and $B_\beta^n(t)$), were values of wavelet energies $E_\mu^n(t)$ and $E_\beta^n(t)$ averaged over the trials.

ERD and ERS corresponding to the right and left hand MI were calculated as integral differences δL_μ^n , δL_β^n and δR_μ^n , δR_β^n between MI trials and the resting state:

$$\delta L_{\mu,\beta}^n = \int_{t \in T} (L_{\mu,\beta}^n(t) - B_{\mu,\beta}^n(t)) dt, \quad (5)$$

$$\delta R_{\mu,\beta}^n = \int_{t \in T} (R_{\mu,\beta}^n(t) - B_{\mu,\beta}^n(t)) dt, \quad (6)$$

with $T = 3$ s standing for the trial length.

2.3 Hierarchical Cluster Analysis (HCA)

One of the goals of this article is to reveal two groups of the subjects corresponding to the different types of motor imagery – VI and KI. We used the hierarchical cluster analysis (HCA), which is a machine learning method that measures the dissimilarity between objects and unites objects into distinct subgroups, or clusters. There are two main types of HCA: agglomerative, which initially considers each element as single-element cluster and combines it with other elements into the bigger clusters, until all elements became members of a cluster, and divisive hierarchical clustering, which is an inverse version of agglomerative clustering. We applied complete-linkage clustering (Defays, 1977), which is the agglomerative clustering method that results in a dendrogram that can give an insight into the clusters hierarchy. This method is also known as a farthest neighbour clustering (Fralely and Raftery, 1998), and the link between two clusters is also considered as a farthest distance between two objects in an M -dimensional feature space with M features describing, in our case, the motor imagery trial of the subject. We calculated the complete-linkage function as:

$$D(X, Y) = \max_{x \in X, y \in Y} d(x, y), \quad (7)$$

where x and y are objects in considered clusters X and Y , respectively, and $d(x, y)$ is the distance between two objects in a feature space calculated using Euclidean metric:

$$d(x, y) = \frac{1}{M} \sqrt{\sum_{i=1}^M (x_i - y_i)^2}, \quad (8)$$

where x_i and y_i are an i -th feature of the x and y objects, respectively.

In present paper, we consider the differences $\delta L_{\mu,\beta}^n$ and $\delta R_{\mu,\beta}^n$ described in previous subsection as features of the MI. We introduced the pair $(\Delta_\mu, \Delta_\beta)$, a two-dimensional space, objects in which describe MI type of all subjects. Here, $\Delta_{\mu,\beta}$ are the wavelet energy differences averaged over the hand type:

$$\Delta_\mu^n = \frac{\delta L_\mu^n + \delta R_\mu^n}{2}, \quad (9)$$

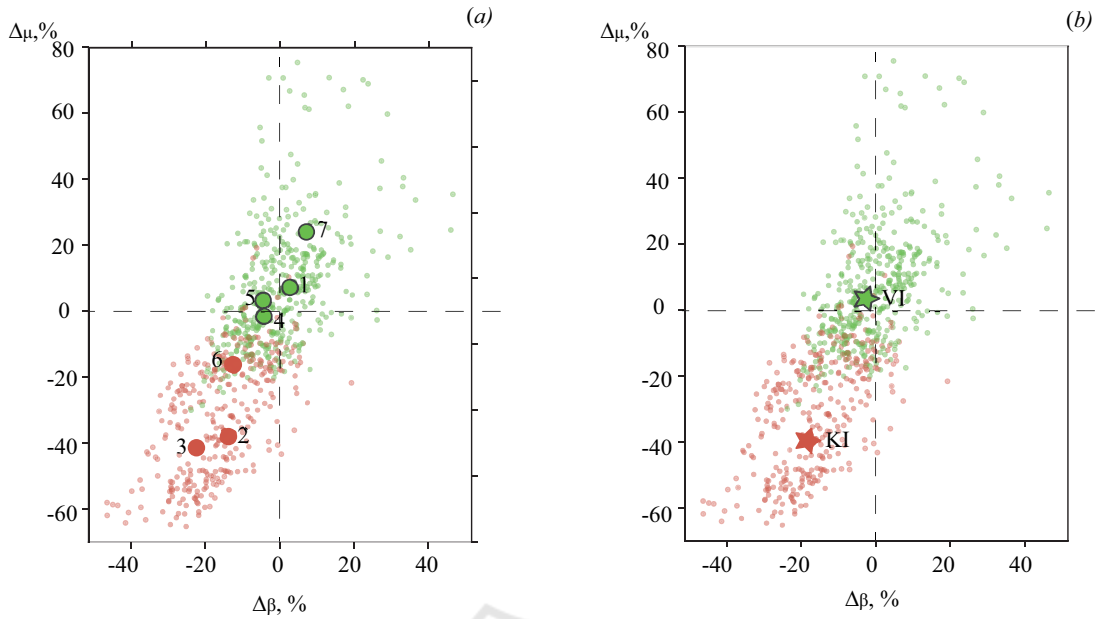


Figure 2: Results of subject clustering to two groups according to the MI type using HCA.

$$\Delta_{\beta}^n = \frac{\delta L_{\beta}^n + \delta R_{\beta}^n}{2}. \quad (10)$$

Finally, due to the high-dimensionality of considering feature space (204 for each limb in case with $N = 102$ MEG channels), we averaged $\Delta_{\mu,\beta}^n$ over the channels:

$$\Delta_{\mu,\beta} = \frac{1}{N} \sum_{n=1}^N \Delta_{\mu,\beta}^n$$

in order to reduce it.

2.4 Artificial Neural Network (ANN)

We used multilayer perceptron (MLP) as an artificial intelligence algorithm to test classifiability of MEG motor imagery pattern with different MI modes. MLP employs feedforward structure with one input and one output layers and several hidden layers. In our study, we used MLP consisted of three hidden layers with 30, 15 and 5 neurons, one neuron on output layer and the hyperbolic tangent sigmoid as an activation function. We applied the Levenberg-Marquardt algorithm as an optimization method, which is a least-squares estimation algorithm based on the idea of the maximum neighbourhood (Übeyli, 2009).

Before the data was fed to the MLP input, it underwent a series of necessary pre-processing. First of all, data was filtered using a low-pass filter with various cutoff frequency ranges. Then, we shuffled the data and splitted it into the training and the test samples that were 75% and 25% of the whole dataset, respectively.

3 RESULTS

Fig. 1 represents the results of HCA, where each dot represents the wavelet energy difference for each MEG channel, each group of subjects has a different colour and big dots are wavelet energy differences averaged over all channels for each subject, representing individual wavelet characteristic of MI. Here, Δ_{μ}^n and Δ_{β}^n are the wavelet coefficients for corresponding frequency bands μ and β , which reflect changes in these frequency bands amplitudes associated with motor imagery for each MEG-channel – in another words, emergence of ERP. The vertical and horizontal dashed lines corresponding to the zero values of Δ_{β}^n and Δ_{μ}^n , separating ERD and ERS for both of the frequency bands.

Thus, all dots placed above the vertical line and to the right from vertical line are representing the MEG channels, where ERS is observed in μ and β - frequency bands, respectively. On the other hand, the negative values of Δ_{β}^n and Δ_{μ}^n are corresponding to the decrease of ERP amplitude, or, in other words, to ERD.

Fig. 2(a) shows the result of HCA clustering of individual MI characteristics of each subject (subjects are represented as big numbered dots). Here we obtained a quite good clustering, allowing us to distinguish two large groups of the subjects, corresponding to the VI and KI, where three subjects belong to the KI group (2, 3 and 6-th, red dots in Fig. 2(a)) and four

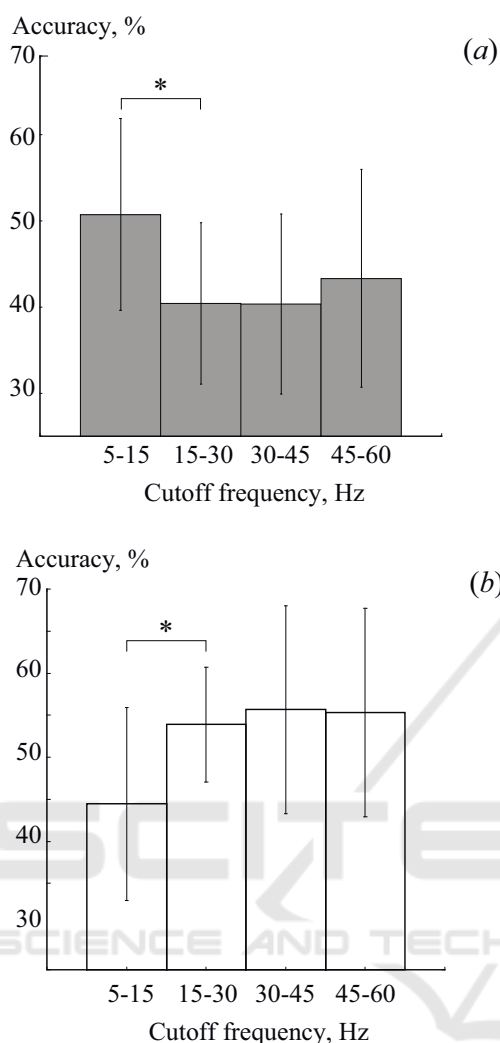


Figure 3: Results of MEG trials classification for (a) KI and (b) VI groups of subjects. Results are presented with the standard deviation.

– to the VI(1, 4, 5 and 7-th, green dots in Fig. 2(a)). As it can be seen from Fig. 2(a), the KI group can be described by decrease of both β and μ rhythms – red dots are mostly placed to the left from the zero value of $\Delta\beta^n$ and below the zero value of $\Delta\mu^n$. It is well-known that ERD in these frequency bands is associated with motor activity, thus we can conclude that subjects in this group were generating motor-related activity during motor imagery.

The other picture is provided by the subjects from VI group. As it was expected, VI is mostly associated with the slight or moderate enhancement of μ -rhythm, which is a sign of visual processing or preparation for movement (Jones et al., 2010). The same changes are observed in the β -band. Moreover, as Fig. 2(b) shows, the subjects from the red group are

generally characterized by well-pronounced ERD in both frequency bands, while the subjects from the green group provided different type behaviour. This close-to-ERS behaviour reflects the main difference between two group of subjects – while the subjects from the red group have a tendency to exercise, the subjects from the green group are mostly prone to the cognitive load.

The next stage of the research included classification of MEG trials with an artificial neural network. Here, we compare the results of the recognition in two groups of subjects selected above and apply low-pass filters with different cutoffs. Fig. 3 shows the results of classification. We can see that using the same low-pass filter results in opposite scenarios in these two groups. For example, here we can see (Fig. 3(a)) that filtering in range 5 – 15 Hz has the most positive effect on the classification accuracy in the VI group. At the same time, the same filter causes significant decrease in the accuracy for the KI subjects (see Fig. 3(b)). Other filter ranges cause sharp drop in classification quality, and then the accuracy does not rise above 45% with increasing filtering cutoffs. Fig. 4 represents the analysis of individual accuracy rates, which evidences that minimal classification accuracy level is reached with [20,40] Hz filtration. These results suggest that low-frequency MEG components are most important in classification of untrained subjects MI, which a conclusion also previously made in our earlier study (Maksimenko et al., 2018).

Fig. 3(b) provides another picture. As it was mentioned above, KI classification results are diametrically opposed to the VI results. Here we can see that the best results are achieved when high-frequency filters are applied. On the contrary, filter with cutoffs 5 – 15 Hz provides 44% accuracy with SD $\pm 12\%$, and the increase in the filtration cutoffs results in accuracy increasing up to $55\% \pm 8$ SD. The individual accuracy for the KI group continues to increase though, reaching it’s maximal value at cutoffs [40, 60] Hz (red circles in Fig.4). Unlike the VI subjects, the KI group produces more MI-related information in the frequency components > 15 Hz. This results can be an evidence that the subjects that prone to KI produce the MI activity similar to preparation to the movement execution.

One of the most topical problem of BCI development is the data reduction or optimization. MEG data consisted of 102 channel recordings is a large dataset, which requires high computing power for it’s processing. With the aim of dataset optimization we reduce number of MEG channels and study the changes in ANN performance. We chose 14 channels located above the motor cortex. Fig. 5 presents results of our

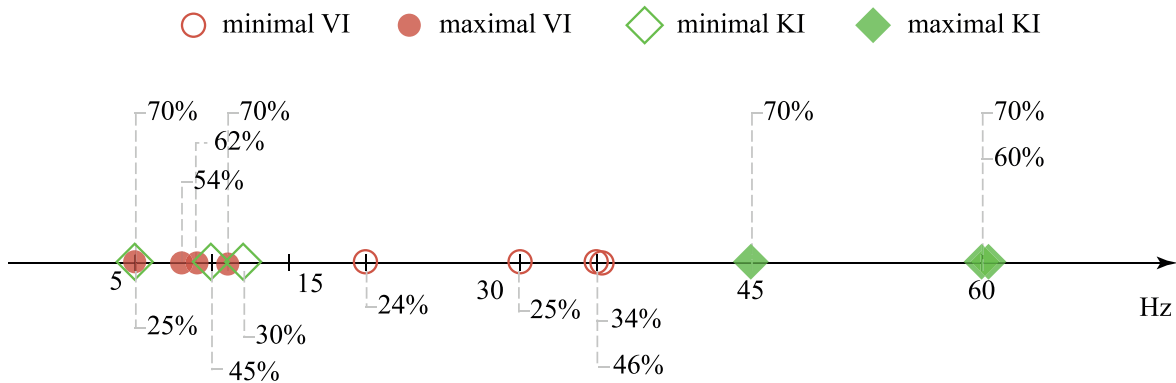


Figure 4: Minimal and maximal accuracy in VI and KI, represented as squares and circles, respectively.

computations.

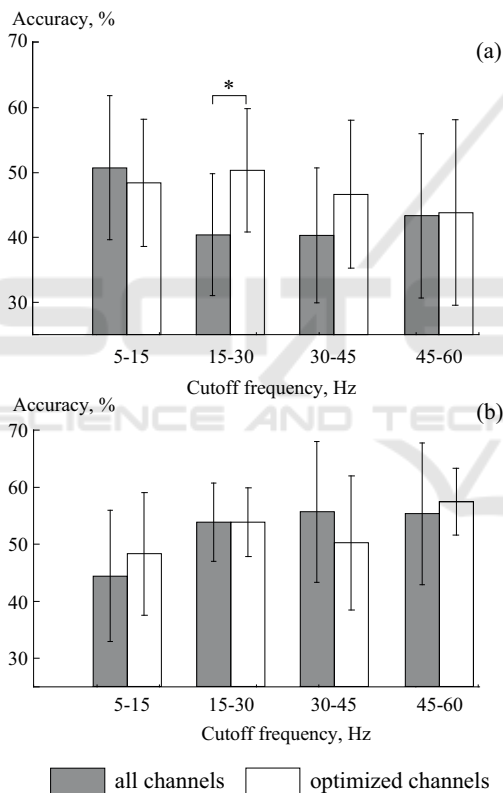


Figure 5: Results of MEG trials classification for optimized and unoptimized dataset for (a) VI and (b) KI groups of subjects. Results are presented with the standard deviation.

For the VI (see Fig. 5(a)) optimization played a positive part in the context of classification performance: one can see that accuracy for cutoff frequency 15 – 30 Hz increased to the level of 5 – 15 Hz. In general, for VI group the optimization of channel set resulted in the increase or at least the absence of significant changes of the classification accuracy. Recent studies (Graimann et al., 2004) of time-frequency

structure of electroencephalography revealed that MI can be pronounced not only in the motor-related cortex, but also in several remote brain areas, which in combination with our results can evidence that VI pattern, which can be pronounced as various brain activity patterns, can emerge in different brain areas.

Returning to the KI group on Fig. 5(b), we can see that optimization did not significantly affect the classification accuracy, even resulting in decrease of neural network performance.

4 CONCLUSION

Classifying motor imagery in untrained subjects into two groups – kinesthetic and visual imagery – is a well-known practice in recent studies. To implement an effective and robust system for classification of MI corresponding to the different limbs, one need to study different scenarios of MI pattern emergence, especially in untrained subjects. A widely known strategy is to study an enhancement and decrease of the sensorimotor rhythm, so-called event-related synchronization and desynchronization – two phenomena related to the motor activity, both real and imagery. In present paper we studied MI of untrained subjects in order to select two types of MI which causes different sensorimotor rhythm pattern and provide a deeper insight into the sensorimotor rhythm dynamics, related to these two MI modes. We show that KI shows better classification results than VI (67% vs 56%) and in general is more pronounced in the context of time-frequency structure of the magnitoencephalographical signal.

At the first stage of our study, we analysed the amplitude changes of event-related potentials in sensorimotor rhythm. Cluster analysis allowed us to divide all subjects into two groups depending on the MI mode. We revealed that the subjects from KI group

demonstrated event-related desynchronization in both β and μ frequency bands, which is expected result considering that the "nature" of the KI pattern is more related to the motor action (Neuper et al., 2005; Guillot et al., 2009). On the contrary, the event-related synchronization was found in the VI subjects.

Then, we enhanced our results using artificial neural network. First, we classified unoptimized magnetoencephalographical dataset with 102 channels and achieved up to 70% accuracy using the low-frequency filter with cutoff below 15 Hz. The same level of accuracy was achieved with KI by applying the high-pass filter with cutoff above 30 Hz. Finally, in order to see how data optimization affects the artificial neural network performance, we selected 14 channels over the motor-related area and revealed no significant changes for KI. On the other hand, the VI group shown the possibility to enhance artificial neural network performance with particular set of channels and frequency cutoffs.

Thus, despite the fact that KI is easier to classify and the KI pattern is more pronounced in time-frequency structure of the MEG signal, there is a possibility to achieve comparable results with the VI. Since the VI mode is more common for untrained subjects, we suggest that obtained results can be useful for implementation of the artificial intelligence systems for MI patterns classification for brain-computer interfaces, exoskeletons, wheelchairs and other robotics devices.

ACKNOWLEDGEMENTS

This work has been supported by Russian Science Foundation (Grant 17-72-30003).

REFERENCES

- Arroyo, S., Lesser, R. P., Gordon, B., Uematsu, S., Jackson, D., and Webber, R. (1993). Functional significance of the mu rhythm of human cortex: an electrophysiological study with subdural electrodes. *Electroencephalography and clinical neurophysiology*, 87(3):76–87.
- Callou, N., Jiang, D., Roberts, R., and Edwards, M. G. (2017). Kinesthetic imagery provides additive benefits to internal visual imagery on slalom task performance. *Journal of Sport and Exercise Psychology*, 39(1):81–86.
- Defays, D. (1977). An efficient algorithm for a complete link method. *The Computer Journal*, 20(4):364–366.
- Duann, J.-R. and Chiou, J.-C. (2016). A Comparison of Independent Event-Related Desynchronization Responses in Motor-Related Brain Areas to Movement Execution, Movement Imagery, and Movement Observation. *PLOS ONE*, 11(9):1–16.
- Ferreira, A., Celeste, W. C., Cheein, F. A., Bastos-Filho, T. F., Sarcinelli-Filho, M., and Carelli, R. (2008). Human-machine interfaces based on EMG and EEG applied to robotic systems. *Journal of NeuroEngineering and Rehabilitation*, 5(1):10.
- Filgueiras, A., Conde, E. F. Q., and Hall, C. R. (2018). The neural basis of kinesthetic and visual imagery in sports: an ale meta- analysis. *Brain imaging and behavior*, 12(5):1513–1523.
- Fraley, C. and Raftery, A. E. (1998). How many clusters? which clustering method? answers via model-based cluster analysis. *The computer journal*, 41(8):578–588.
- Frolov, A. A., Mokienko, O., Lyukmanov, R., Biryukova, E., Kotov, S., Turbina, L., Nadareyshvily, G., and Bushkova, Y. (2017). Post-stroke rehabilitation training with a motor-imagery-based brain-computer interface (BCI)-controlled hand exoskeleton: a randomized controlled multicenter trial. *Frontiers in neuroscience*, 11:400.
- Graimann, B., Huggins, J. E., Levine, S. P., and Pfurtscheller, G. (2004). Toward a direct brain interface based on human subdural recordings and wavelet-packet analysis. *IEEE Transactions on Biomedical Engineering*, 51(6):954–962.
- Guillot, A., Collet, C., Nguyen, V. A., Malouin, F., Richards, C., and Doyon, J. (2009). Brain activity during visual versus kinesthetic imagery: an fmri study. *Human brain mapping*, 30(7):2157–2172.
- Hanakawa, T. (2016). Organizing motor imageries. *Neuroscience research*, 104:56–63.
- Jones, S. R., Kerr, C. E., Wan, Q., Pritchett, D. L., Hämäläinen, M., and Moore, C. I. (2010). Cued spatial attention drives functionally relevant modulation of the mu rhythm in primary somatosensory cortex. *Journal of Neuroscience*, 30(41):13760–13765.
- Kübler, A., Nijboer, F., Mellinger, J., Vaughan, T. M., Pawelzik, H., Schalk, G., McFarland, D. J., Birbaumer, N., and Wolpaw, J. R. (2005). Patients with ALS can use sensorimotor rhythms to operate a brain-computer interface. *Neurology*, 64(10):1775–1777.
- La Touche, R., Grande-Alonso, M., Cuenca-Martínez, F., González-Ferrero, L., Suso-Martínez, L., and Paris-Alemany, A. (2018). Diminished Kinesthetic and Visual Motor Imagery Ability in Adults With Chronic Low Back Pain. *PM&R*.
- Maksimenko, V. A., Pavlov, A., Runnova, A. E., Nedaivozov, V., Grubov, V., Koronovskii, A. A., Pchelintseva, S. V., Pitsik, E., Pisarchik, A. N., and Hramov, A. E. (2018). Nonlinear analysis of brain activity, associated with motor action and motor imaginary in untrained subjects. *Nonlinear Dynamics*, 91(4):2803–2817.
- McFarland, D. J. and Wolpaw, J. R. (2005). Sensorimotor rhythm-based brain-computer interface (BCI): feature selection by regression improves performance. *IEEE Transactions on Neural Systems and Rehabilitation Engineering*, 13(3):372–379.

- Mehler, D. M. A., Williams, A. N., Krause, F., Lührs, M., Wise, R. G., Turner, D. L., Linden, D. E. J., and Whitaker, J. R. (2019a). The BOLD response in primary motor cortex and supplementary motor area during kinesthetic motor imagery based graded fMRI neurofeedback. *Neuroimage*, 184:36–44.
- Mehler, D. M. A., Williams, A. N., Krause, F., Lührs, M., Wise, R. G., Turner, D. L., Linden, D. E. J., and Whitaker, J. R. (2019b). The BOLD response in primary motor cortex and supplementary motor area during kinesthetic motor imagery based graded fMRI neurofeedback. *NeuroImage*, 184:36–44.
- Meng, J., Zhang, S., Bekyo, A., Olsoe, J., Baxter, B., and He, B. (2016). Noninvasive electroencephalogram based control of a robotic arm for reach and grasp tasks. *Scientific Reports*, 6:38565.
- Mirza, I. A., Tripathy, A., Chopra, S., D'Sa, M., Rajagopalan, K., D'Souza, A., and Sharma, N. (2015). Mind-controlled wheelchair using an EEG headset and arduino microcontroller. In *Technologies for Sustainable Development (ICTSD), 2015 International Conference on*, pages 1–5. IEEE.
- Morlet, D., Peyrin, F., Desseigne, P., Touboul, P., and Rubel, P. (1993). Wavelet analysis of high-resolution signal-averaged ECGs in postinfarction patients. *Journal of Electrocardiology*, 26(4):311–320.
- Murphy, D. P., Bai, O., Gorgey, A. S., Fox, J., Lovegreen, W. T., Burkhardt, B. W., Atri, R., Marquez, J. S., Li, Q., and Fei, D.-Y. (2017). electroencephalogram-Based Brain-computer interface and Lower-Limb Prosthesis control: A case study. *Frontiers in neurology*, 8:696.
- Neuper, C., Scherer, R., Reiner, M., and Pfurtscheller, G. (2005). Imagery of motor actions: Differential effects of kinesthetic and visual-motor mode of imagery in single-trial eeg. *Cognitive brain research*, 25(3):668–677.
- Nijboer, F., Morin, F. O., Carmien, S. P., Koene, R. A., Leon, E., and Hoffmann, U. (2009). Affective brain-computer interfaces: Psychophysiological markers of emotion in healthy persons and in persons with amyotrophic lateral sclerosis. In *2009 3rd International Conference on Affective Computing and Intelligent Interaction and Workshops*, pages 1–11. IEEE.
- Norman, S. L., McFarland, D. J., Miner, A., Cramer, S. C., Wolbrecht, E. T., Wolpaw, J. R., and Reinkensmeyer, D. J. (2018). Controlling pre-movement sensorimotor rhythm can improve finger extension after stroke. *Journal of neural engineering*, 15(5):56026.
- Öztürk, N. and Yilmaz, B. (2018). Discrimination of Rest, Motor Imagery and Movement for Brain-Computer Interface Applications. In *2018 Medical Technologies National Congress (TIPTEKNO)*, pages 1–4. IEEE.
- Penaloza, C. I., Alimardani, M., and Nishio, S. (2018). Android feedback-based training modulates sensorimotor rhythms during motor imagery. *IEEE Transactions on Neural Systems and Rehabilitation Engineering*, 26(3):666–674.
- Ranky, G. N. and Adamovich, S. (2010). Analysis of a commercial EEG device for the control of a robot arm. In *Proceedings of the 2010 IEEE 36th Annual Northeast Bioengineering Conference (NEBEC)*, pages 1–2. IEEE.
- Tacchino, G., Gandolla, M., Coelli, S., Barbieri, R., Pedrocchi, A., and Bianchi, A. M. (2017). EEG Analysis during active and assisted repetitive movements: evidence for differences in neural engagement. *IEEE Transactions on Neural Systems and Rehabilitation Engineering*, 25(6):761–771.
- Übeyli, E. D. (2009). Combined neural network model employing wavelet coefficients for eeg signals classification. *Digital Signal Processing*, 19(2):297–308.
- Victorino, J., Noirhomme, Q., Lulé, D., Kleih, S. C., Chatelle, C., Halder, S., Demertzi, A., Bruno, M.-A., Gosseries, O., Vanhauzenhuysse, A., and Others (2015). Improving EEG-BCI analysis for low certainty subjects by using dictionary learning. In *Signal Processing, Images and Computer Vision (STSIVA), 2015 20th Symposium on*, pages 1–7. IEEE.
- Yi, W., Qiu, S., Wang, K., Qi, H., He, F., Zhou, P., Zhang, L., and Ming, D. (2016). EEG oscillatory patterns and classification of sequential compound limb motor imagery. *Journal of neuroengineering and rehabilitation*, 13(1):11.
- Yu, T., Xiao, J., Wang, F., Zhang, R., Gu, Z., Cichocki, A., and Li, Y. (2015). Enhanced motor imagery training using a hybrid BCI with feedback. *IEEE Transactions on Biomedical Engineering*, 62(7):1706–1717.